Magnetic and electric antennas synergy for partial discharge measurements in gas-insulated substations

Power flow and reflection suppression

Mier, Christian; Rodrigo Mor, Armando; Vaessen, Peter; Lathouwers, André

DOI
10.1016/j.ijepes.2022.108530

Publication date
2023

Document Version
Final published version

Published in
International Journal of Electrical Power and Energy Systems

Electrical Power and Energy Systems 144 (2023) 108530

Contents lists available at ScienceDirect

International Journal of Electrical Power and Energy Systems

journal homepage: www.elsevier.com/locate/ijepes

Magnetic and electric antennas synergy for partial discharge measurements in gas-insulated substations: Power flow and reflection suppression

Christian Mier [a,*], Armando Rodrigo Mor [b], Peter Vaessen [a], André Lathouwers [a]

[a] Delft University of Technology, High Voltage Technology Group, Mekelweg 4, 2628 CD Delft, The Netherlands
[b] Universitat Politècnica de València, Instituto de Tecnología Eléctrica, Camino de Vera s/n, 46022 Valencia, Spain

ARTICLE INFO

Keywords:
partial discharges
PD sensors
GIS
pulse overlapping
UHF antenna
magnetic antenna

ABSTRACT

One of the main difficulties in measuring partial discharges (PD) in gas-insulated substations (GIS) is the overlapping of pulses at the sensor's location, which distorts the pulse resolution and the charge estimation. This research presents a new method called "synergy," which identifies and suppresses reflections using magnetic and electric antennas in the very-high frequency range. By scaling the antennas' outputs and adding them, it is possible to segregate forward and backward pulses. Additionally, by multiplying the electric and magnetic signals, the power flow of the pulses is obtained, which identifies the propagation direction and the location of discontinuities in the transmission path. The synergy method is evaluated in three scenarios: a fully matched test bench using a calibrated pulse, a full-scale GIS using a calibrated pulse, and a full-scale GIS using a PD defect. The results showed that the pulse reflections can be eliminated from the incident pulse, improving the charge calculation when the pulses overlap. The output of this research represents an improvement for PD monitoring in GIS, exhibiting a tool for better defect localization, pulse wave shape construction, charge estimation, and possible interference rejection.

1. Introduction

An accepted method for insulation diagnosis is partial discharge (PD) measurements, and in many cases, it is a requirement in the acceptance protocol [1]. The PD charge magnitude is not only an important parameter for insulation degradation assessment but also harmonizes readings from different sensors: the charge magnitude reading is independent of the sensor characteristics if adequately calibrated and measured. The IEC 60270 [2] is a standard for "conventional methods" where the device under test is electrically small; PD analysis in test objects that electrically behave as distributed parameters devices is out of the scope of the standard due to the complicated resonances and pulse reflection phenomena. References [3,4] demonstrate that non-conventional detectors, dealing with conducted signals and in a specific frequency range, can provide calibrated charge magnitudes; however, the pulse superposition, which distorts the PD measurements, is still a concern in gas-insulated substation (GIS).

Reference [6] demonstrates that PDs in SF_6 have a few nanoseconds duration, having a wavelength many times smaller than GIS length. Therefore, the GIS behaves as a waveguide for PD pulses in which, depending on the frequency, it has three propagation modes: transverse electromagnetic (TEM), transverse electric (TE), and transverse magnetic (TM); due to the complex propagation in the last two modes, the PD charge can only be measured in TEM mode [7,8]. Since the TEM mode propagation follows the transmission line (TL) theory, each GIS section (spacers, T-connection, bushing, etc.) can be represented as a discontinuity where pulse reflections occur [9–11]. Due to the GIS geometry, its TEM mode occurs below the ultra-high frequency (UHF) range; therefore, sensors measuring in the very-high frequency (VHF) range and below are suitable for PD charge estimation.

Reference [12] shows a novel PD measuring system for GIS consisting of a magnetic antenna, and [4] demonstrates that magnetic and electric (UHF sensor) antennas, working in the VHF range (TEM mode frequency), can be calibrated in a GIS, and be able to estimate the PD

Abbreviations: PD, partial discharges; GIS, gas-insulated substations; TE, transverse electric; TM, transverse magnetic; TEM, transverse electromagnetic; TL, transmission line; UHF, ultra-high frequency; VHF, very-high frequency; V2I, voltage double integral; EM, electromagnetic; PF, power flow; BW, bandwidth; TRF, transformation filter; CB, circuit breaker; HFCT, high frequency current transformer.

* Corresponding author.
E-mail address: c.mierescurra@tudelft.nl (C. Mier).

https://doi.org/10.1016/j.ijepes.2022.108530
Received 11 April 2022; Received in revised form 21 June 2022; Accepted 1 August 2022
Available online 12 August 2022

charge. There are several methods for PD charge estimation [13]; however, the voltage double integral (V2I) method is the most suitable for non-flat narrow band sensors [14]. It is demonstrated that the charge of the magnetic [15] and the electric antenna [4] can be correctly estimated using the V2I method.

This publication reveals that having a magnetic and electric antenna placed at the same longitudinal GIS position allows the identification of the incident and the reflected pulses propagating in the TEM mode (below the UHF range). Two approaches are proposed for the reflection discrimination with an extension of the V2I method. The discrimination methods are compared and evaluated in three different test setups: a matched test bench, a full-scale GIS with a calibrated pulse, and the full-scale GIS with a PD defect. Additionally, the power flow of the propagated pulse is shown for each test setup, which clearly identifies the propagation direction and helps with the PD interpretation.

2. Pulse propagation in GIS

2.1. Power flow

When a PD occurs, an electromagnetic (EM) wave propagates in all directions, and given that a single-phase enclosed GIS behaves as a coaxial waveguide, the PD propagates in two directions in the waveguide axis. The EM propagation direction is independent of the PD polarity and can be characterized using the Poynting vector ($\bar{s}$). The Poynting vector represents the power flow per unit area; if it is integrated over the coaxial cross-section results in the voltage and current product (1), where PF is the power flow, $\vec{e}$ is the electric field, $\vec{h}$ is the magnetic field, $\vec{a}$ is the cross-section, V is the voltage and I is the current; an example is illustrated in Fig. 1 using cylindrical coordinates (r,φ,z). Having a magnetic and an electric antenna, the PD current and voltage can be measured, and thus, the power flow can be obtained in a GIS.

$$PF = \int_A \vec{e} \times \vec{h} \cdot d\vec{a} = VI \tag{1}$$

When a transmission line is not matched, the measured signal is formed by the incident pulse followed by forward and backward components. This article refers to the forward component as the incident pulse and the reflections that occur before the observation point, and the backward component as the reflections that occur after the observation point. Equations (2) and (3) represent the voltages and currents when the TL has discontinuities, where V^+ and V^- are the forward and backward voltage pulses, respectively; I^+ and I^- are the forward and backward current pulses, respectively; Z_1 and Z_2 are the impedances before and after the discontinuity; z is the distance from the discontinuity to the observation point, c is the speed of light in the medium, being $2z/c$ the time delay between the incident and the reflected pulse; and Γ is the reflection coefficient. The reflection equations and the Poynting vector can identify the backward component from the forward component.

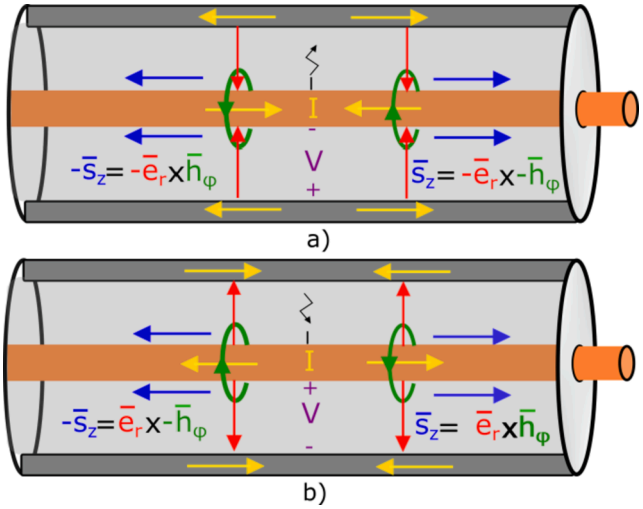

Fig. 1. Poynting vector $\bar{s}$ for a) positive and b) negative discharge.

$$V^-(z,t) = \Gamma V^+(t + 2z/c) \text{ where } \Gamma = \frac{Z_2 - Z_1}{Z_2 + Z_1} \tag{2}$$

$$I^+(z,t) = \frac{V^+(z,t)}{Z_0} \text{ and } I^-(z,t) = -\frac{V^-(z,t)}{Z_0} \tag{3}$$

The signal's instantaneous power cannot be recovered with GIS PD sensors due to their narrow bandwidth (BW); however, it is possible to represent the signal's power flow. Forward and backward pulses can be distinguished using the power flow equation (4), where the first term is the incident and all forward pulses, and the second term is all backward pulses, having opposite polarity compared to the forward component. An overlapping happens when the time delay between backward and forward signals is shorter than the pulse duration; this overlapping can be avoided by eliminating the reflections using the magnetic and electric antennas, as shown in the next subchapters. Being able to distinguish the reflected pulses improves the PD charge estimation, PD wave shape, and defect location.

$$PF(z,t) = V(z,t)I(z,t) = \underbrace{\frac{V^{+^2}(z,t)}{Z_0}}_{forward} - \underbrace{\frac{\Gamma^2 V^{+^2}(t + 2z/c)}{Z_0}}_{backward} \tag{4}$$

2.2. Elimination of pulse reflections

The previous chapter showed that forward and backward pulses can be distinguished by the polarity difference; therefore, by superimposing the measured PD current and voltage, the backward pulses can be reduced. Equations (5) and (6) show the electric and magnetic antennas measurements with the forward and backward components. If one of the outputs, the electric, for instance, is scaled (α) to match the magnetic output, according to (3) the backward component changes polarity and results in (7). Therefore, adding the magnetic and the scaled electric output results in a forward component increment and a backward component elimination (8). Equation (8) is an ideal situation where the scale factor perfectly matches one antenna to the other. The following sections show two proposed scale factors to reduce reflections.

$$V_e(t) = V_e^+(t) + V_e^-(t) \tag{5}$$

$$V_m(t) = V_m^+(t) + V_m^-(t) \tag{6}$$

$$\alpha V_e(t) = V_m^+(t) - V_m^-(t) \tag{7}$$

$$V_m(t) + \alpha V_e(t) = 2V_m^+(t) \tag{8}$$

Before introducing the scale factors, it is worth mentioning the antennas' impulse response in the frequency and time domain. In the VHF range, the electric and magnetic antennas can be represented as a single-pole transfer function ([16,17]) where the higher cutoff frequency is above the VHF range. To ensure that only TEM mode frequencies are measured, the signals of the sensors are filtered, giving the transfer function in (9), where V_o is the output voltage, I_{pd} is the measured PD current, k is the calibration constant, ω_0 is the lower cutoff frequency, and $H(s)$ is the low-pass filter transfer function. The electric antenna's PD voltage relates to the PD current by the local characteristic impedance (Z_0) of the GIS [4], which is included in the k factor in (9). Reference [5] shows that PD in SF_6 have a rise time below 1 ns, which means that in the VHF range, the PD pulse can be seen as a Dirac delta pulse with a Laplace domain magnitude equal to the charge Q and a time delay t_0, resulting in (10) by using (9) and solving for the output voltage. To simplify the evaluation, a 1st order filter was chosen and a Dirac delta

pulse when t_0=0, giving the time domain function in (11).

$$\frac{V_o(s)}{I_{pd}(s)} = \underbrace{\frac{ks}{s/\omega_0 + 1}}_{sensor} \underbrace{H(s)}_{filter} \tag{9}$$

$$V_o(s) = Qe^{-st_0}\frac{ks}{s/\omega_0 + 1}H(s) \tag{10}$$

$$V_o(t) = Q\frac{k\omega_0^2\omega_f}{\omega_0 - \omega_f}e^{-\omega_0 t} - Q\frac{k\omega_f^2\omega_0}{\omega_0 - \omega_f}e^{-\omega_f t} \tag{11}$$

2.2.1. Peaks scale factor

One proposal is to match the magnetic and electric antennas' measured peaks: from equation (11), we can see that the peak occurs when t=0, resulting in (12); therefore, the peak's ratio between the electric and magnetic antennas is the factor C_{pk} and is equal to (13). Now, if the backward component of the electric sensor (V_e) is subtracted from the scaled magnetic sensor's backward component (V_m C_{pk}), the resultant backward pulse (V_{em}) is obtained (14). Note in (14) that if the filters' cutoff frequencies are equal (ω_{fe}=ω_{fm}) and the sensors' low cutoff frequencies are also identical (ω_{0e}=ω_{0m}), then the reflections are eliminated. The filters corner frequencies can be selected as wished; however, ω_0 depends on the self-inductance and parasitic capacitance of the magnetic and electric antennas. The inductance and capacitance of the sensors can be manipulated by the physical design (as in a directional coupler), with the risk of altering other antenna parameters.

$$V_o(0) = V_{peak} = Qk\omega_0\omega_f \tag{12}$$

$$C_{pk} = \frac{V_{peak-e}}{V_{peak-m}} = \frac{k_e\omega_{0e}\omega_{fe}}{k_m\omega_{0m}\omega_{fm}} \tag{13}$$

$$\begin{aligned} C_{pk}V_m(t)^- - V_e(t)^- &= V_{em}(t)^- \\ &= Q\left(\frac{k_e\omega_{0e}\omega_{0m}\omega_{fe}}{\omega_{0m} - \omega_{fm}}e^{-\omega_{0m}t} - \frac{k_e\omega_{0e}^2\omega_{fe}}{\omega_{0e} - \omega_{fe}}e^{-\omega_{0e}t}\right. \\ &\quad \left. + \frac{k_e\omega_{fe}^2\omega_{0e}}{\omega_{0e} - \omega_{fe}}e^{-\omega_{fe}t} - \frac{k_e\omega_{0e}\omega_{fe}\omega_{fm}}{\omega_{0m} - \omega_{fm}}e^{-\omega_{fm}t}\right) \end{aligned} \tag{14}$$

2.2.2. Transformation filter scale factor

An alternative method is to process the signal of one of the sensors in a way that both antennas have the same transfer function, eliminating the opposite polarity reflections. To mimic one antenna's output signal into the other, a convolution is done using the antenna's transfer function (the one to be scaled) and a transformation filter (TRF): equation (15) shows the transformation of the magnetic output ($V_{m\to e}$), where $H_{e/m}$ represents the TRF. Equation (16) shows the resultant pulse by superimposing the electric output and the scaled magnetic output (the same procedure can be done to mimic the magnetic antenna's output ($V_{e\to m}$)). The TRF is the antenna's transfer function to be mimicked over the antenna's transfer function to be scaled (17). Equation (18) represents the TRF using electric parameters, where C_1 and C_2 are the coupling and parasitic capacitances of the electric antenna, M and L_s are the coupling inductance and self-inductance of the magnetic antenna, and R is the load for both antennas. The transformation filter can be analog or digital: the first involves construction difficulties, while the second requires more signal processing, and is the one used in this research.

$$V_{m\to e}(t) = \frac{1}{2\pi j}\int_0^t e^{st}\left(V_m(s)^* H_{e/m}(s)\right)ds \tag{15}$$

$$V_{em}(t) = V_e(t) + V_{m\to e}(t) \tag{16}$$

$$H_{e/m}(s) = \frac{V_e(s)}{V_m(s)} = \frac{k_e\left(\frac{s}{\omega_{0m}} + 1\right)}{k_m\left(\frac{s}{\omega_{0e}} + 1\right)} \tag{17}$$

$$H_{e/m}(s) = \frac{C_1RZ_0\left(\frac{sL_s}{R} + 1\right)}{M(sC_2R + 1)} \tag{18}$$

It is not mentioned in previous equations, but it is fundamental to have the minimum time lag between antennas, ideally zero. In either method (peaks and TRF), the electric and magnetic antennas must be located at the same longitudinal position at the GIS, so the propagated pulse is induced in both sensors simultaneously. Reference [17] shows that the magnetic antenna's shield delays the sensed signal, so it must be corrected to ensure that the electric and magnetic antenna's signals are in phase. The peaks and TRF scale factors have practical advantages and disadvantages, and their efficacy is shown in the results section.

2.2.3. Charge estimation

The previous subchapter demonstrates two methods for reflections suppression; since both methods superimpose the voltage and current measurements, the resultant pulse charge is also affected. According to [14], the double-time integral of the output voltage is equal to the charge and the calibration constant, and reducing the integration limit to the pulse second zero crossing (t_0) results in the approximation in (19). Additionally, [14] shows that the calibration constant equals the transfer function when the frequency approaches zero (20). Equation (21) is an extension when multiple sensors' outputs are superimposed, where V_{em} is the addition of both sensors. In the filter transformation method (applied to the magnetic sensor), the calibration constant of the magnetic antenna results equal to the electric antenna constant (22); hence, the V_{em} charge estimation results in Q_{tf}, given by (23) (a comparable conclusion is obtained transforming the electric output). The peaks method changes the charge in a similar way: when one of the sensor's output in (21) is scaled by the peaks factor (C_{pk}), the calibration constant must be affected by the same factor resulting in the approximated charge Q_{pk}, shown in (24). If both antennas have the same cutoff frequency then k_mC_{pk}=k_e, giving the same results as in (23). In the following sections, the use of the electric and magnetic antennas for reflection elimination and segregation is identified by the author through the paper as "synergy".

$$\int_0^{t_0}\int_0^{t_0} V_o(t)dt \approx Qk\to Q \approx \frac{1}{k}\int_0^{t_0}\int_0^{t_0} V_o(t)dt \tag{19}$$

$$k \approx lim\left|\frac{G(\omega)}{\omega}\right|_{\omega\to 0} when\ \omega \neq 0 \tag{20}$$

$$\int_0^{t_0}\int_0^{t_0} (V_m(t) + V_e(t))dt \approx Q(k_e + k_m) \to Q \approx \frac{1}{k_e + k_m}\int_0^{t_0}\int_0^{t_0} V_{em}(t)dt \tag{21}$$

$$k_m \approx lim\left|\frac{G_m(\omega)^* H_{e/m}(\omega)}{\omega}\right|_{\omega\to 0} \approx k_e \tag{22}$$

$$Q_{tf} \approx \frac{1}{2k_e}\int_0^{t_0}\int_0^{t_0} V_{em}(t)dt \tag{23}$$

$$\begin{aligned} \int_0^{t_0}\int_0^{t_0} (V_m(t)C_{pk} + V_e(t))dt &\approx Q_{pk}(k_e + k_mC_{pk}) \to Q_{pk} \\ &\approx \frac{1}{k_e + k_mC_{pk}}\int_0^{t_0}\int_0^{t_0} V_{em}(t)dt \end{aligned} \tag{24}$$

3. Experimentation

The power flow and reflection elimination method require the PD current and voltage measurements, which can be done with a magnetic and an electric antenna. The magnetic sensor used for all experiments was a shielded balanced magnetic antenna [18] presented in Fig. 2: this antenna has a middle gap in the outer shield, rejecting a higher amount of common-mode noise [19]. The electric antennas used for the test bench (Fig. 3 a) and the full-scale GIS (Fig. 3 b) were commercial sensors, having the dimensions presented in Fig. 3. Three different test setups are proposed: a matched test bench, where no unintended reflections occur; a full-scale GIS with a calibrator and transition cones, in which the propagated pulse is subjected to different GIS discontinuities; and a full-scale GIS with a PD defect, evaluating a real scenario. The experiments in the test bench and the full-scale GIS were performed using an ultra-fast pulse calibrator (<1 ns rise time), and all the test setups were measured with a 2 GHz Tektronix MSO58 oscilloscope.

3.1. Matched Test bench

A fully matched test bench was used to have pulse propagation without reflections. The test bench consists of a GIS section connected to a pulse source where all elements are matched to 50 Ω, and transition cones were used (a full explanation of the test bench construction can be found in [20]) to allow a smooth transition from the source to the GIS. It is mandatory for the synergy that both sensors are synchronized in time; hence, the GIS section has two mounting holes at the same longitudinal position, ensuring that the propagated pulse is measured simultaneously in both sensors. Fig. 4 shows a picture of the test bench with the two mounting holes.

The test bench experiment aims to test the synergy in an ideal environment free of unwanted discontinuities. To evaluate the pulse power flow, a pulse was consecutively injected in both directions, with both polarities, where the opposite cone was short-circuited and open-circuited (OC). The reflection elimination and charge estimation were evaluated with no pulse overlap, having an open circuit 596 cm away from the sensors (extending the test bench with a coaxial cable), and with pulse overlap, having a short circuit 76 cm apart from the sensors, using a 10 ns width pulse.

3.2. Full-scale GIS using a calibrated pulse

In previous experiment no unplanned reflections were produced due to the almost perfect 50 Ω matching of all elements; on the other hand, a full-scale GIS consists of several sections: spacers, bushings, circuit breaker (CB), "T" section, etc., each of them acting as a discontinuity to the propagated PD pulse, which results in multiple reflections. In this experiment, the same fast calibrator pulse was connected to the GIS through a transition cone, where the pulses were measured in the GIS section indicated in Fig. 5: 6.1 meters away from the injection point and 4.1 meters from the CB. Since the transition cone and the GIS do not match the calibrator's 50 Ω impedance, part of the signal is reflected. A directional coupler was used to measure the transmitted input signal: the reference charge is calculated by subtracting the forward coupled charge with the reverse coupled charge (a complete explanation is shown in [4,21]). The test setup is represented in Fig. 6.

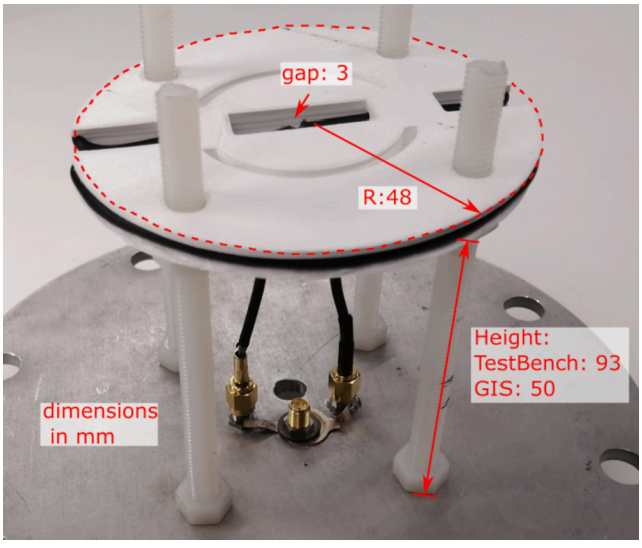

Fig. 2. Top-view and dimensions of the balanced magnetic antenna.

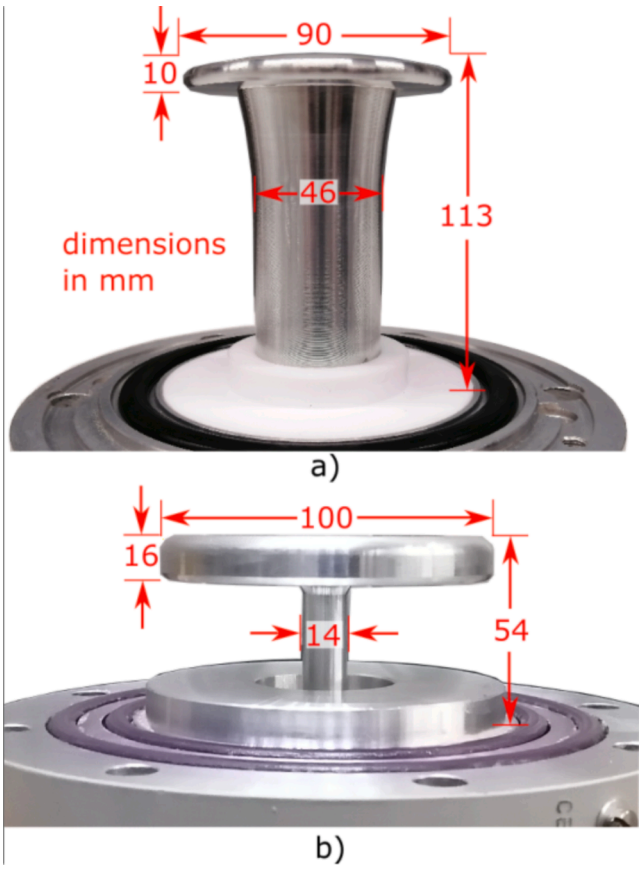

Fig. 3. Photos with dimensions in mm for the electric antenna in the a) test bench and b) GIS.

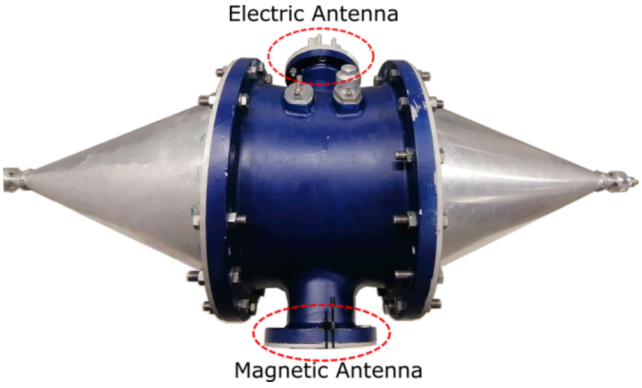

Fig. 4. Picture of the test bench.

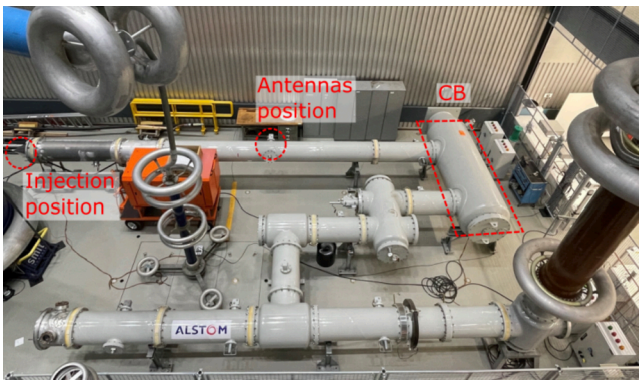

Fig. 5. Full-scale GIS top view indicating the sensors and injection positions.

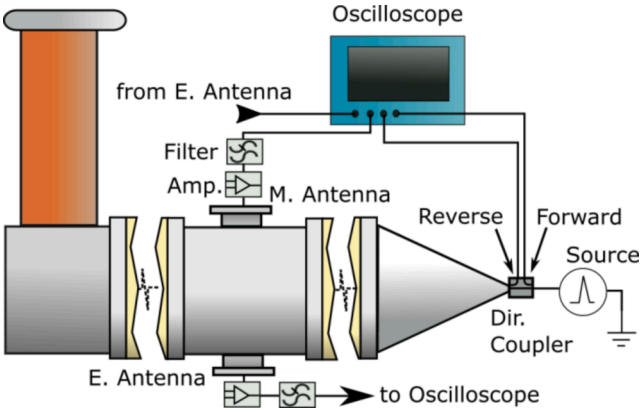

Fig. 6. Test setup for a full-scale GIS using a calibrator pulse.

3.3. Full-scale GIS using a PD defect

The test's purpose is to evaluate, using real PD, the forward and backward pulses segregation, the power flow, and the estimated charge with and without the synergy method. To evaluate the accuracy of the PD charge estimation method, the antennas' outputs must be compared with a reference measurement. Since the GIS behaves as a transmission line, the "conventional method" can not be used ([1–3]). Hence, a different procedure was employed: before reaching the GIS enclosure, the PD current is forced to flow in a rod where a broadband HFCT (high-frequency current transformer) is coupled, allowing the charge calculation by means of the PD current integration [13].

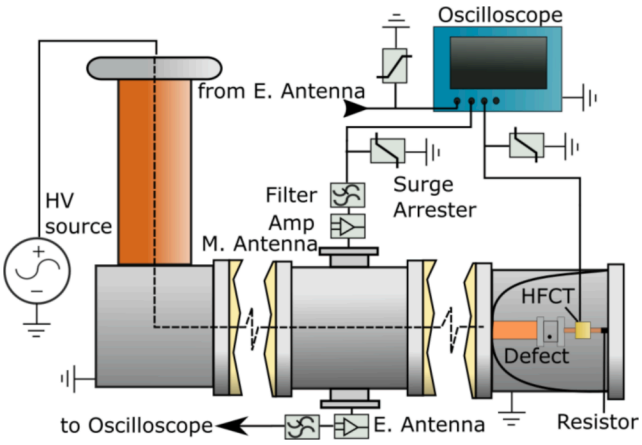

Fig. 7. Test setup for a full-scale GIS using a PD defect.

Table 1
Magnetic and electric antennas' electric parameters in the test bench and GIS.

	Test bench	GIS
C_1 [pF]	0.49	0.30
Z_0 [Ω]	50	70
R [Ω]	50	50
M [nH]	0.72	0.90
C_2 [pF]	10	17
L_s [nH]	160	160

The same full-scale GIS from the previous subchapter was used but without a transition cone (Fig. 7), where the source was a jumping particle PD defect in a 3 bar (relative pressure) SF_6 test-cell. The GIS was energized with an HV source up to the PD's inception, and the test-cells' electrodes were connected to the GIS' HV conductor and the enclosure via a rod and a 75 Ω damping resistor. The PD current pulses were measured with a 4 kHz-1 GHz BW HFCT and electric and magnetic antennas, in which their outputs were connected to the oscilloscope through a 25 dB, 1 GHz voltage amplifier and a 190 MHz low-pass filter. For safety reasons, 1 GHz surge arresters were connected in parallel to the oscilloscope input. The antennas and the source were in the same positions as the previous test setup.

4. Results and discussion

This chapter presents and discusses the power flow, reflection elimination, and charge estimation results using the test setups presented in previous chapter. Reference [4] shows that the PD charge estimation requires a calibration process where the calibration constant (k) is found; additionally, it is necessary to find the antennas' cutoff frequencies (ω_0) to eliminate the reflections using the TRF method. Table 1 and Table 2 show the electric parameters and the transfer function constants, respectively. The electric parameters can be obtained using the techniques in [17] and [4], excluding C_2. The electric antenna's parasitic capacitance can be obtained in the test bench by measuring the frequency response; however, this is not the case for the full-scale GIS where C_2 was obtained with finite element method simulation. In the following charge estimations, the TRF method is evaluated twice: by scaling the magnetic and electric antenna. In the case of the peaks method, the normalization of any antenna results in the same values.

4.1. Matched Test bench

4.1.1. Power flow results

Fig. 8 presents the measured pulses for different input pulses and discontinuities: a) is a positive polarity pulse propagating from the left-hand side in an open circuited test bench, b) is a positive polarity pulse propagating from the right-hand side in a short-circuited test bench, c) is the same as a) but with a negative polarity pulse, d) is the same as b) but with a negative polarity pulse. The magnetic antenna's output is scaled with the C_{pk} factor for better visualization. Using the measured pulses in Fig. 8, Fig. 9 shows the power flow for each combination: a) is the PF for Fig. 8 a) and c), and b) is for Fig. 8 b) and d). The individual electric or magnetic antennas' outputs (Fig. 8) does not provide the propagation direction: the incident polarity, the reflection coefficient, and the pulse

Table 2
Magnetic and electric antennas' transfer function parameters in the test bench and GIS.

	Test bench	GIS
k_m [nΩs]	0.72	0.90
k_e [nΩs]	1.22	1.10
ω_{0m} [rad/s]	$3.1\text{x}10^8$	$3.1\text{x}10^8$
ω_{0e} [rad/s]	$2.0\text{x}10^9$	$1.2\text{x}10^9$

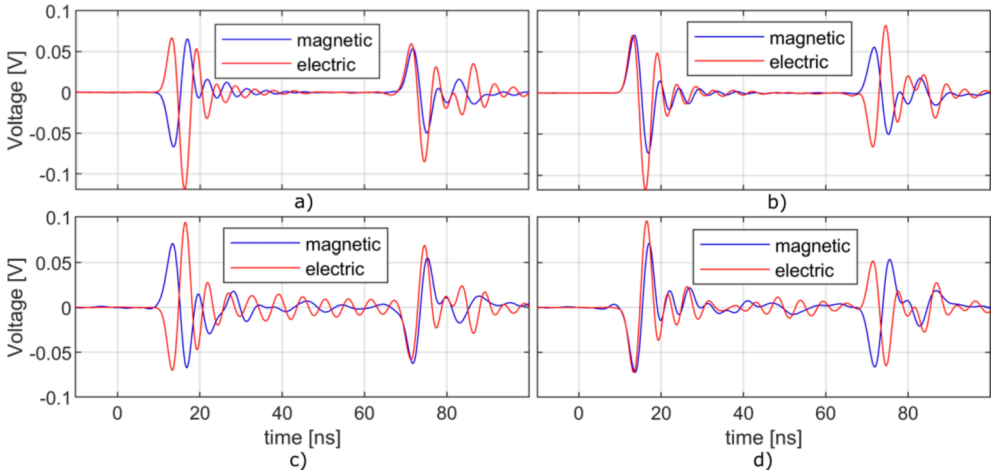

Fig. 8. Electric and scaled magnetic antennas measurements where: a) left propagated positive polarity pulse in an open-circuited test bench, b) right propagated positive polarity pulse in a short-circuited test bench, c) same as a) but with a negative polarity pulse, d) is the same as b) but with a negative polarity pulse [22].

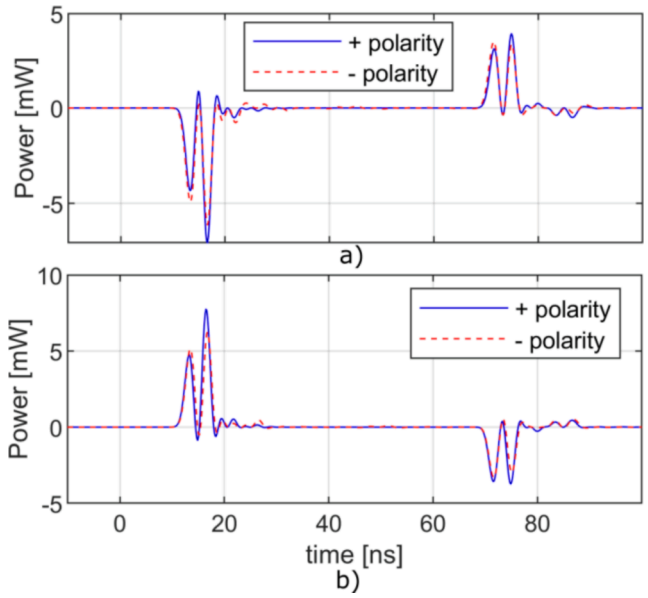

Fig. 9. a) Power flow for both polarity pulses in an open circuit test bench, propagated from the left, and b) power flow for both polarity pulses in a short circuit test bench, propagated from the right [22].

direction affect the pulse polarity. Fig. 9 shows that the power flow correctly identifies the direction of the propagation independently of previous variables: the power flow analysis provides a better tool for PD defects localization, reducing the number of sensors. Furthermore, knowing the pulse direction might help to discriminate interferences coming into the GIS.

4.1.2. Reflection elimination and charge estimation results

This section presents the reflection elimination and the resultant charge results using the peaks and the transformation filter methods. Fig. 10 shows the measurements when a short circuit is 76 cm away from the sensors: a) magnetic and electric antennas measured pulses with discontinuity and compared with matched pulses, b) discerned incident and reflected pulses using the peak method and compared with a matched pulse, and c) is the same as b) but using the TRF method applied to the electric antenna. Fig. 10 a) shows that the measured waveforms are distorted compared to the matched case: since the discontinuity is a short-circuit, the magnetic antenna has a constructive

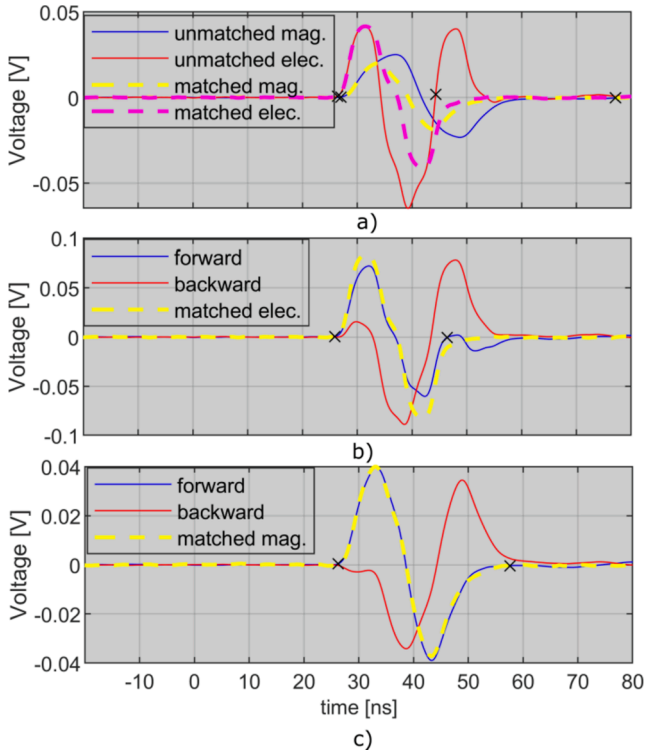

Fig. 10. Short-circuited test bench at 76 mm: a) unmatched and matched magnetic and electric measured pulses; b) incident and reflected pulses using the peaks method, and matched electric pulse; and c) incident and reflected pulses using the TRF method, and matched magnetic pulse [22]. The black crosses indicate the zero crossings used for the charge calculation.

superposition while the electric sensor has a destructive one. In b) and c), the forward pulse approximates the matched case, having a better result when applying the TRF method than the peak method because the superposition affects the peak values. The reflected pulse is well segregated, coinciding the space delay (5.3[ns]*30[cm/ns]) with the 2x76 [cm] discontinuity distance. Please note that in b), the matched electric measurement is used for comparison since the peak's constant is applied to the magnetic sensor. In c), the matched magnetic output is used because the TRF method is applied to the electric sensor.

In the non-overlapping situation (Fig. 11), the transformation filter

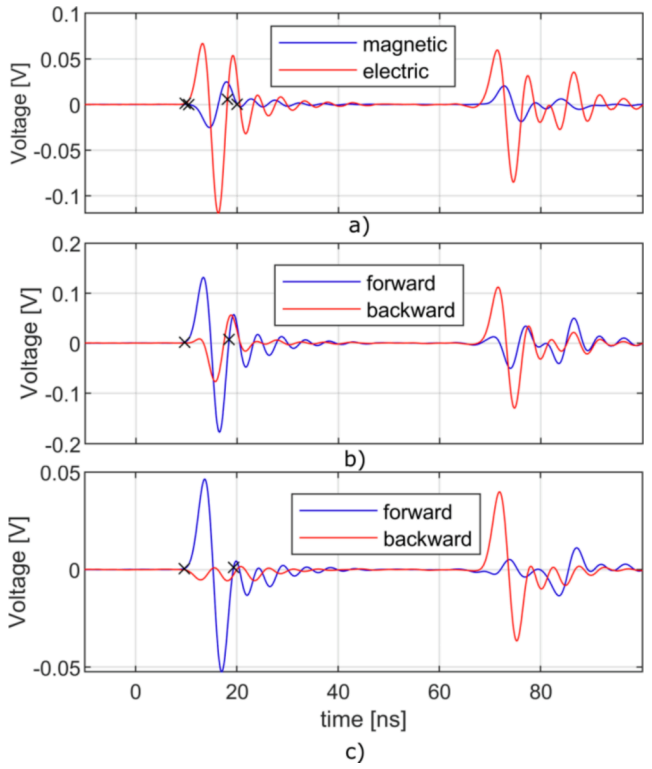

Fig. 11. Test bench open-circuited at 596 mm: a) magnetic and electric antennas measured pulses, b) incident and reflected pulses using the peaks method, and c) incident and reflected pulses using the TRF method [22].

Table 3
Charge estimation error without and with synergy with a discontinuity at 596 and 76 cm.

	Error @ 76 cm (pulse overlap)	Error @ 596 cm (no pulse overlap)
Magnetic	89 %	-15 %
Electric	-60 %	-15 %
Peaks	-18 %	-23 %
TRF Electric	4.2 %	-0.2 %
TRF Magnetic	6.2 %	-29 %

also shows a better reflection elimination because of the cutoff frequencies difference between antennas which affects the peaks method. Table 3 shows the calculated charge errors without and with synergy methods when the discontinuity is 596 cm (no pulse overlap) and 76 cm (pulse overlap) apart from the antennas. The charge estimation is improved using the synergy method when the pulse is overlapped, from above 60% to below 7% error (in the TRF case). By improving the pulse wave shape, a better PD identification can be obtained [23].

4.2. Full-scale GIS using a calibrated pulse

Fig. 12 shows the measurements performed in a full-scale GIS using the fast calibrator pulse. The oscillography of the synergy in the following sections was performed with the TRF method since it showed better reflection reduction. Fig. 12 a) shows the measured magnetic and electric pulses, b) shows the extracted forward and backward pulses, and c) shows the calculated power flow. As shown in b), the resulted forward pulse is cleaner than the raw measurements in a); however, multiple pulses remain: the incident pulse propagates through multiple discontinuities before reaching the antennas (forward reflections), and the synergy method is limited to backward reflections. This concept is more

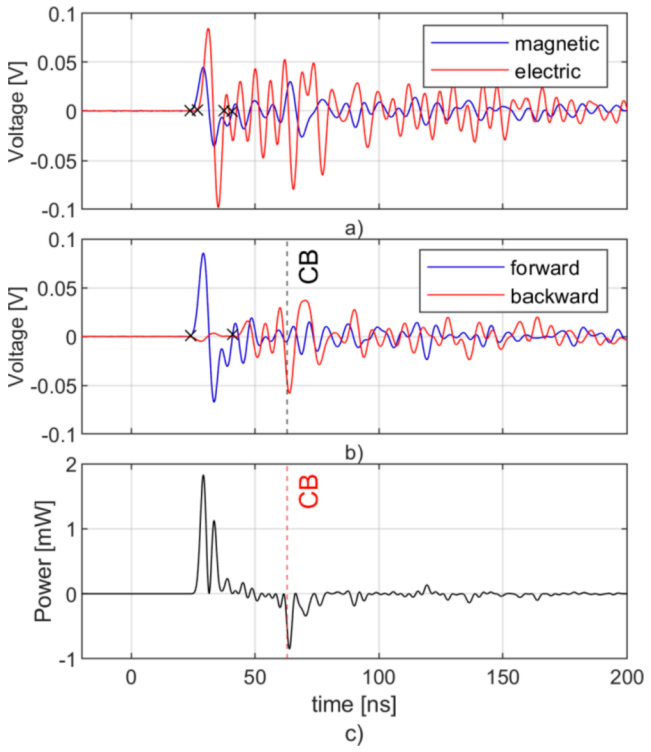

Fig. 12. a) measured electric and magnetic antennas, b) TRF synergy with CB location, c) PF with CB location. The crosses and circle markers identify the zeros crossing used for the charge calculation [22].

evident in the power flow plot: all positive pulses correspond to the incident and forward reflections, and negative pulses correspond to backward reflections. The location of the circuit breaker is indicated with a dashed line in Fig. 12 b) and c), corresponding to a significant change of impedance in the GIS. Table 4 shows the calculated charge errors without and with synergy: due to the isolated sensors' position relative to the discontinuities, the backward reflections do not affect the measured incident pulses. The charge error increased for the peak's method because of the cutoff frequency difference between antennas.

4.3. Full-scale GIS using a PD defect

This section shows the measurements and results performed in the full-scale GIS with a jumping particle PD defect. Fig. 13 presents the waveforms of one of the measured PD: a) shows that the reference pulse (measured with the HFCT) has low oscillation due to the low lower-cutoff frequency and its broad BW, allowing the charge calculation using the current integration; c) shows the discerned forward and backward pulses by applying the TRF synergy method, giving a clearer pulse compared to the raw measurements in b); and d) shows the PD's power flow, where the location of the circuit breaker is identified. In Fig. 14, the charges of the 200 PD pulses are compared between the reference (x-axis) and the antennas' outputs and the synergy (y-axis): a better estimation is obtained when the reflections are eliminated.

Table 4
Charge estimation error for the magnetic and electric antennas measurements and synergy methods.

	Error
Magnetic	-1.2 %
Electric	-15 %
Peaks	-17 %
T. Filter Electric	-8.5 %
T. Filter Magnetic	-9.5 %

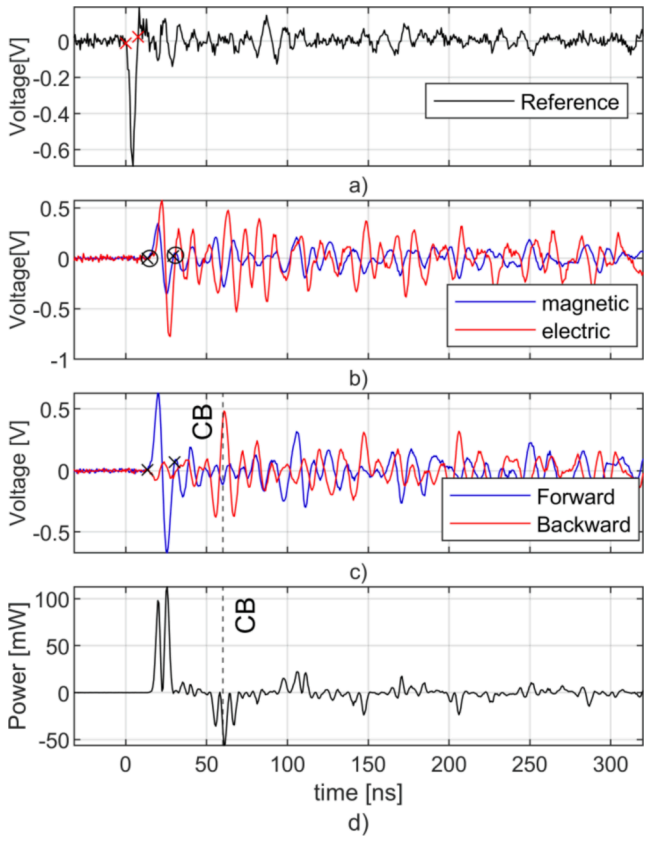

Fig. 13. a) HFCT (reference) measurement, b) electric and magnetic antennas measurement, c) TRF synergy with CB location, d) PF with CB location. The crosses and circle markers identify the zeros crossing used for the charge calculation [22].

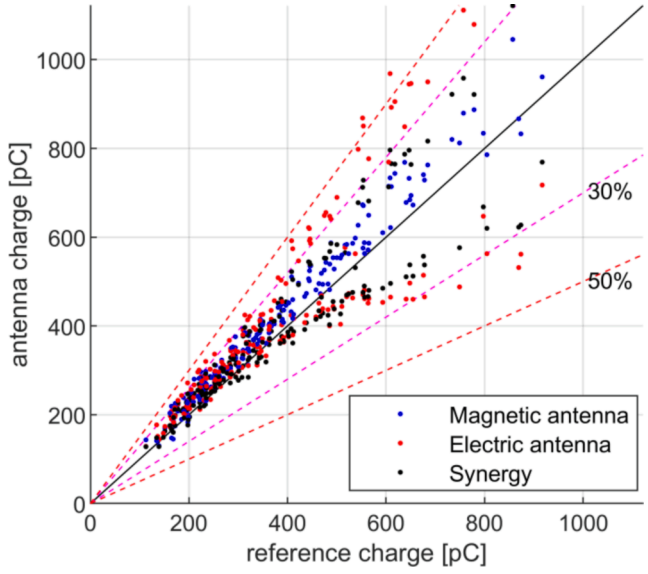

Fig. 14. Antennas and synergy charges compared with reference charges for 200 PDs. Dashed lines show 30% and 50% charge estimation error boundaries [22].

Table 5
Percentile of PDs charges below 30 % of error for the magnetic and electric antennas, and synergy methods

	Percentile below 30% error
Magnetic	98 %
Electric	78 %
Peaks	97 %
TRF Electric	99.0 %
TRF Magnetic	87 %

Table 5 shows the percentage of PD that falls below the 30 % of error: the transformation filter applied to the electric antenna resulted in a more accurate charge estimation than when applied to the magnetic antenna because of the magnetic antenna's better accuracy compared to the electric antenna.

Previous results showed that the synergy method helps in the charge calculation accuracy when multiple reflections exist. Moreover, the PF plot clearly shows the forward and backward PD pulses, where the CB reflection results in the same position as in section 4.2, giving a unique pattern dependent on the PD location and the GIS discontinuities. By recognizing the pattern, it is possible to distinguish multiple PD sources or reflections of a single pulse; also, a different pattern is expected for non-TEM interference measurements, indicating a potential for interference rejection.

5. Conclusions

The present research aims to determine a method for PD reflections suppression in GIS using an electric and a magnetic antenna. This study presented two scaling factors for forward and backward pulse propagation segregation, helping to identify the pulse power flow, and improve the wave shape and charge estimation. The synergy method was tested in three test setups showing good charge estimation for different pulses and discontinuities, where the transformation filter method showed a better reflection suppression than the peaks method. The power flow accurately located discontinuities in the GIS and test bench, even for overlapped pulses. The synergy approach, besides the charge estimation improvement, has the possibility of interference discrimination, which motivates further research to assess the synergy method in noisy environment resembling on-line substations.

CRediT authorship contribution statement

Christian Mier: Conceptualization, Methodology, Formal analysis, Investigation, Writing – original draft, Visualization, Writing – review & editing. **Armando Rodrigo Mor:** Conceptualization, Writing – review & editing, Supervision, Project administration. **Peter Vaessen:** Writing – review & editing, Supervision. **André Lathouwers:** Writing – review & editing.

Declaration of Competing Interest

The authors declare that they have no known competing financial interests or personal relationships that could have appeared to influence the work reported in this paper.

Data availability

My data can be found in a public repository which is referenced in the article.

Acknowledgements

This project 19ENG02 FutureEnergy has received funding from the EMPIR programme co-financed by the Participating States and from the European Union's Horizon 2020 research and innovation programme. Funder ID: 10.13039/100014132.

References

[1] WG D1.33, "Guidelines for Unconventional Partial Discharge Measurements," *CIGRE*, pp. 1–58, 2010.
[2] IEC 60270, "Partial Discharge Measurements," 2015.
[3] Cavallini A, Montanari GC, Tozzi M. PD apparent charge estimation and calibration: A critical review. IEEE Trans. Dielectr. Electr. Insul. 2010;17(1):198–205.
[4] Mier C, Rodrigo Mor A, Castro L, Vaessen P. Magnetic and electric antennas calibration for partial discharge charge estimation in gas-insulated substations. Int. J. Electr. Power Energy Syst. 2022;vol. 141, no. January:108226.
[5] Reid AJ, Judd MD, Stewart BG, Fouracre RA. Partial discharge current pulses in SF6 and the effect of superposition of their radiometric measurement. J. Phys. D. Appl. Phys. 2006;39(19):4167–77.
[6] Judd MD, Farish O, Hampton BF. The excitation of UHF signals by partial discharges in GIS. IEEE Trans. Dielectr. Electr. Insul. 1996;3(2):213–28.
[7] Behrmann G, Franz S, Smajic J, Tanasic Z, Christen R. UHF PD signal transmission in GIS: Effects of 90° bends and an L-shaped CIGRE step 1 test section. IEEE Trans. Dielectr. Electr. Insul. 2019;26(4):1293–300.
[8] Ohtsuka S, Teshima T, Matsumoto S, Hikita M. Relationship between PD induced electromagnetic wave measured with UHF method and charge quantity obtained by PD current waveform in model GIS. In: in *Electrical Insulation and Dielectric Phenomena*; 2006. p. 615–8.
[9] Imagawa H, et al. PD signal propagation characteristics in GIS and its location system by frequency components comparison. IEEE Trans. Power Deliv. 2001;16(4):564–70.
[10] M. Hikita, "Fundamental principles and application of diagnosis for GIS using partial discharge measurements," *Proc. 2011 Int. Conf. Electr. Eng. Informatics, ICEEI 2011*, no. July, pp. 11–16, 2011.
[11] Hikita M, Ohtsuka S, Wada J, Okabe S, Hoshino T, Maruyama S. Propagation properties of PD-induced electromagnetic wave in 66 kV GIS model tank with L branch structure. IEEE Trans. Dielectr. Electr. Insul. 2011;18(5):1678–85.
[12] A. Rodrigo Mor, L. Castro Heredia, and F. Muñoz, "A Novel Approach for Partial Discharge Measurements on GIS Using HFCT Sensors," *Sensors*, vol. 18, no. 12, p. 4482, Dec. 2018.
[13] Mor AR, Morshuis PHF, Smit JJ. Comparison of charge estimation methods in partial discharge cable measurements. IEEE Trans. Dielectr. Electr. Insul. 2015;22(2):657–64.
[14] A. Rodrigo-Mor, F. A. Muñoz, and L. C. Castro-Heredia, "Principles of charge estimation methods using high-frequency current transformer sensors in partial discharge measurements," *Sensors (Switzerland)*, vol. 20, no. 9, 2020.
[15] A. Rodrigo Mor, L. C. Castro Heredia, and F. A. Muñoz, "A magnetic loop antenna for partial discharge measurements on GIS," *Int. J. Electr. Power Energy Syst.*, vol. 115, no. June 2019, p. 105514, 2020.
[16] Kurrer R. Teilentladungsmessung im Gigaherts-Frequencbereich an SF6-isolierten Schaltanlagen. Stuttgart 1997.
[17] Mier C, Mor AR, Vaessen P. Design and Characterization of a Magnetic Loop Antenna for Partial Discharge Measurements in Gas Insulated Substations. IEEE Sens. J. 2021;21(17):18618–25.
[18] Libby LL. Special Aspects of Balanced Shielded Loops. Proc. IEEE 1946;34(9):641–6.
[19] Carobbi CFM, Millanta LM. Analysis of the Common-Mode Rejection in the Measurement and Generation of Magnetic Fields Using Loop Probes. IEEE Trans. Instrum. Meas. 2004;53(2):514–23.
[20] Mier C, Mor AR. Test Bench and Frequency Response of a Magnetic Antenna used in GIS PD Measurements. no. 2021;2:269–72.
[21] Mier C, Mor AR. "Partial Discharge Charge Estimation In Gas Insulated Substations Using Electric and Magnetic Antennas", in *IEEE*. International Conference on Dielectrics 2022;2022:1–4.
[22] C. Mier, "Mag&ElecSynergy." Mendeley Data, V2.
[23] Alvarez F, Ortego J, Garnacho F, Sanchez-Uran MA. A clustering technique for partial discharge and noise sources identification in power cables by means of waveform parameters. IEEE Trans. Dielectr. Electr. Insul. 2016;23(1):469–81.